ACS OMEGA

http://pubs.acs.org/journal/acsodf

Article

Highly Efficient Sulfur and Nitrogen Codoped Graphene Quantum Dots as a Metal-Free Green Photocatalyst for Photocatalysis and Fluorescent Ink Applications

Tamizharasan Selvakumar, Muralidharan Rajaram, Abirami Natarajan, Leelavathi Harikrishnan, Kumarasamy Alwar, and Arulmozhi Rajaram*

Cite This: *ACS Omega* 2022, 7, 12825−12834

Read Online

ACCESS | Metrics & More | Article Recommendations

ABSTRACT: The demand for modern organic pollutant treatment has prompted the development of environmentally acceptable photocatalytic processes. In this work, we report novel nitrogen and sulfur codoped graphene quantum dot (S,N-GQD) based photocatalysts and fluorescent ink for the first time. For the degradation of organic dyes under visible irradiation, a hydrothermal technique was employed to generate S,N-GQD green nanomaterials. The synthesized samples were examined using XRD, HR-TEM, EDX, FT-IR, PL, and UV−vis spectroscopy. UV-DRS was used to determine the energy band gap of S,N-GQDs, and it was obtained to be around ∼2.54 eV. To explore the catalytic behavior of the produced S,N-GQDs as green nanomaterials, organic dyes (i.e., crystal violet and Alizarin yellow) have been used as a reference dye in this study. Using several radical scavenging agents, the photocatalytic mechanism was examined. This novel photocatalyst offers a promising alternative for the breakdown of organic pollutants. Moreover, these S,N-GQDs can also be used as fluorescent ink for imaging purposes and security reasons.

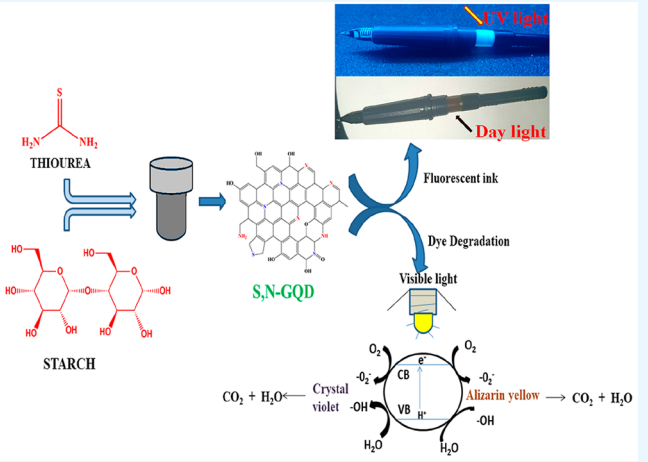

1. INTRODUCTION

Water pollution caused by colors from diverse industries such as textiles, leather, paper, medications, beauty products, printing, and dye production has become a global issue that has harmed both human and aquatic life.[1,2] As per the United Nations World Water Development Report (UV WWDR), over 748 million people are unaware that there is a shortage of safe drinking water, and the amount of water needed by manufacturing industries has continued to increase 400% since the turn of the century, with another 400% increase expected by 2050.[3,4] Dyes are a major source of water pollution, with 1−15% of the dye being lost as a pollutant during the dyeing process.[5] Wastewater is typically made as a result of human actions such as use, agricultural production, and industrialization as a result of population growth.[6,7] These issues continuously occur and might have a stronger impact in the future.[8,9]

Graphene belongs to the famous carbon-based nanomaterials. They have received a lot of attention because of their significant electrical and mechanical properties. It can be used to improve properties in host materials for various applications.[10] Carbon nanomaterials have low toxicity, physical and chemical stability, high biocompatibility, easy products, and low cost.[11] A new zero-dimensional carbon nanomaterial, graphene quantum dots (GQDs), has a lateral size of fewer than 10 manometers.[12−14] GQDs are attracting much attention due to their use in various fields such as biosensors, drug delivery, cellular imaging, solar cells, wastewater treatment, and water splitting.[15−21] GQDs have been synthesized using a variety of strategies, including "top-down" and "bottom-up" approaches.[22,23] Larger (micrometer) structures are made into smaller (nanometer-sized) quantum dots in the top-down technique.[24] The top-down method has some disadvantages, such as minimum quantum yield, expensive equipment, and toxic starting materials, and controlling the size of dots is difficult. The bottom-up method

Received: January 5, 2022
Accepted: March 22, 2022
Published: April 4, 2022

https://doi.org/10.1021/acsomega.2c00092
ACS Omega 2022, 7, 12825−12834

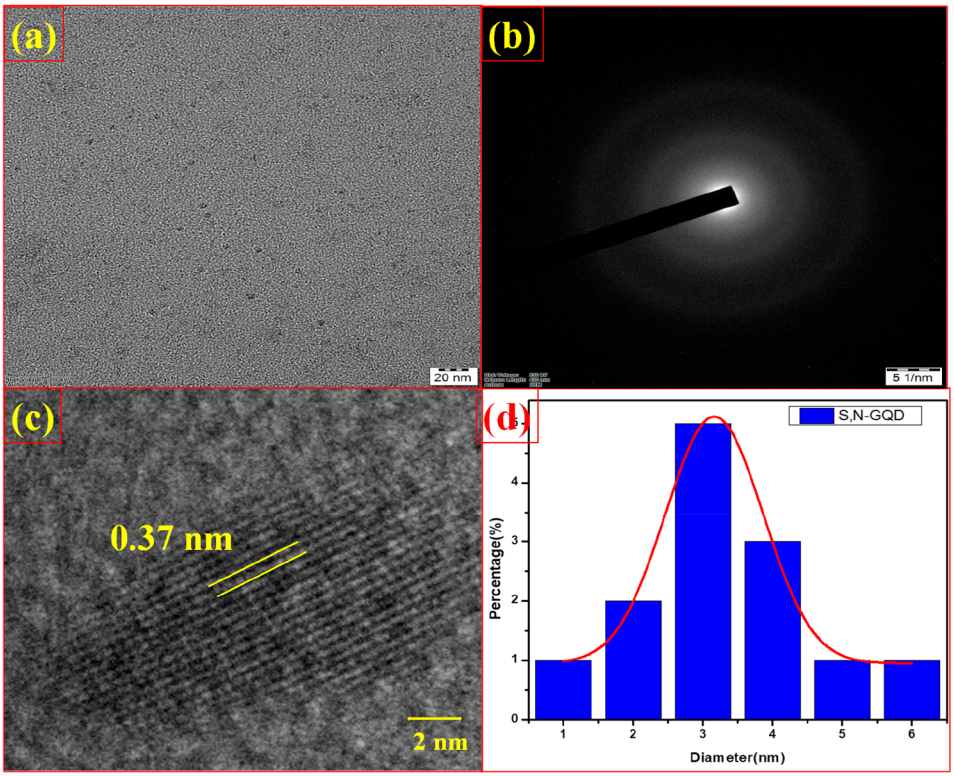

Figure 1. (a) TEM image for S,N-GQDs, (b) SAED pattern of S,N-GQDs, (c) HRTEM image and graphitic lattice fringes of S,N-GQDs, and (d) size distribution of as-prepared S,N-GQDs.

is simple in controlling the morphology and size distribution.[25−28] Pure graphene quantum dots (GQDs) are not a good choice for photocatalytic degradation. To make the GQDs effective, doping them with heteroatoms such as boron,[29] nitrogen,[30] sulfur,[31] and fluorine[32] improves the fluorescence properties and catalytic activity compared to that of undoped GQDs. Therefore, the functionalization with N and S, on graphene quantum dot preparation and characterization, becomes significant for photocatalysis and fluorescent ink applications, and currently, researchers are working on a simple and environmentally friendly approach to make highly luminescent GQDs.[33−36] Several environmentally friendly GQD-making methods have been reported, including the use of low-cost plant extracts, fruit juices, hair, milk, and culinary waste as carbon precursors, and have received more attention. However, these precursor materials and synthesis methods require sophisticated equipment, time-consuming sample preparation, and expensive reagents. Hence, S,N-GQD green nanomaterial preparation methods are preferable because they offer many benefits, including high signal output, simplicity, ease of monitoring, quick response, and cost effectiveness. As a result, establishing a simple, sustainable fluorescent green nanomaterial is highly essential.[37,38]

In this paper, we report an easy, safe, and efficient bottom-up method for the synthesis of metal-free S, N codoped GQD green nanomaterial by using Starch as a Carbon precursor and thiourea as a sulfur and nitrogen dopant. Synthesized S, N codoped GQD was used as a photocatalyst for degradation of crystal violet and alizarin yellow organic dyes under Visible light conditions. It degraded up to ∼91% for crystal violet and ∼64% for alizarin yellow dye solutions as measured by UV−vis spectroscopy and we also looked at undoped GQDs for crystal violet dye degradation and found that it has a degradation rate of up to 56% only. these confirms in this work dopant plays an important rule and also it has very efficient catalyst compared to previously reported works. This demonstrates that the dopant plays a major role in this activity and S, N-GQDs are also excellent for making undetectable blue color emitting fluorescent ink pens for imaging and security applications due to their high fluorescent characteristics and photostability. It confirms that the catalyst is extremely efficient compared to earlier studies.

2. RESULTS AND DISCUSSION

2.1. Characterization of the S,N-GQDs. The TEM images of the synthesized S,N-GQDs are given in Figure 1a, and they reveal the morphology of S,N-GQDs as spherical in shape with particle size ranging between 1 and 6 nm. The average size of S,N-GQDs is around 3.13 nm, as shown in the TEM histogram (Figure 1d). Then the HRTEM image of S,N-GQDs shows the presence of graphitic fringes and the *d*-spacing value of ∼0.37 nm, and it is marked with the yellow line as shown in Figure 1c. The SAED pattern of S,N-GQDs is shown in Figure 1b, and the white circle-ring-like structure clearly indicates the very low crystallinity of S,N-GQDs.

XRD analysis was used to assess the crystallographic information on the synthesized S,N-GQDs, and the diffraction pattern is shown in Figure 2. The XRD pattern of S,N-GQDs appears as a weak broad peak centered around $2\theta = 24°$, and its *d*-spacing value is around ∼0.37 nm along the (002) direction. The interlayer spacing in the 002 plane is significantly better than that of conventional bulk graphite (0.344 nm). This supports the hypothesis that the synthesized S,N-GQDs have a graphitic structure with a small amount of amorphous carbon. The amorphous carbon could be

https://doi.org/10.1021/acsomega.2c00092
ACS Omega 2022, 7, 12825−12834

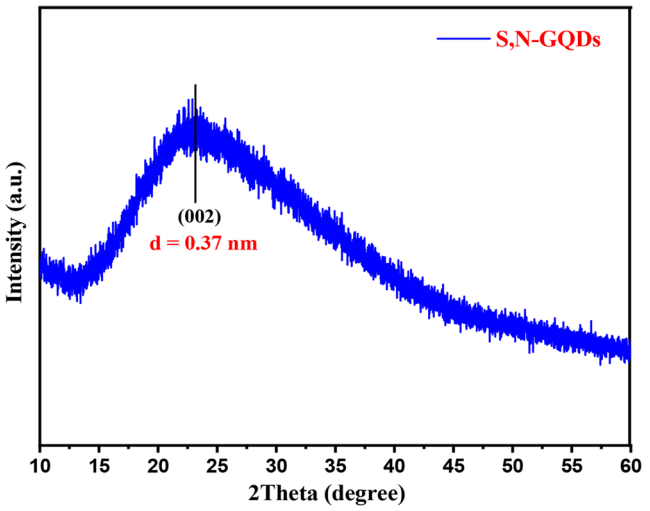

Figure 2. XRD pattern of S,N-GQDs.

attributable to the surface functionalities of S,N-GQDs that have been fabricated and agrees well with the previously reported works.[53−56]

EDX measurements also confirmed the presence of expected elements in the analyzed structures. Figure 3a shows the amount of each element detected by EDX measurement. Carbon, nitrogen, sulfur, and oxygen were discovered on the surface of the as-prepared S,N-GQDs, along with the atomic percentages of the components provided in Table 1. The EDX data indicate the existence of nitrogen and sulfur in the S,N-GQDs, thus confirming the formation of sulfur and nitrogen doping in S,N-GQDs.

The TEM-mapping image shown in Figure 3b demonstrates the presence of all the elements (i.e., C, O, N, and S) that are present in the S,N-GQDs. Also, as shown in this figure, the concentrations of the elements present in the S,N-GQDs indicate that N, O, and S elements have lower concentrations than the C element. This confirms that carbon is a major element present on the surface of the graphitic structure.

S,N-GQD surface functional groups were investigated through Fourier transform infrared (FT-IR) analysis. Infrared

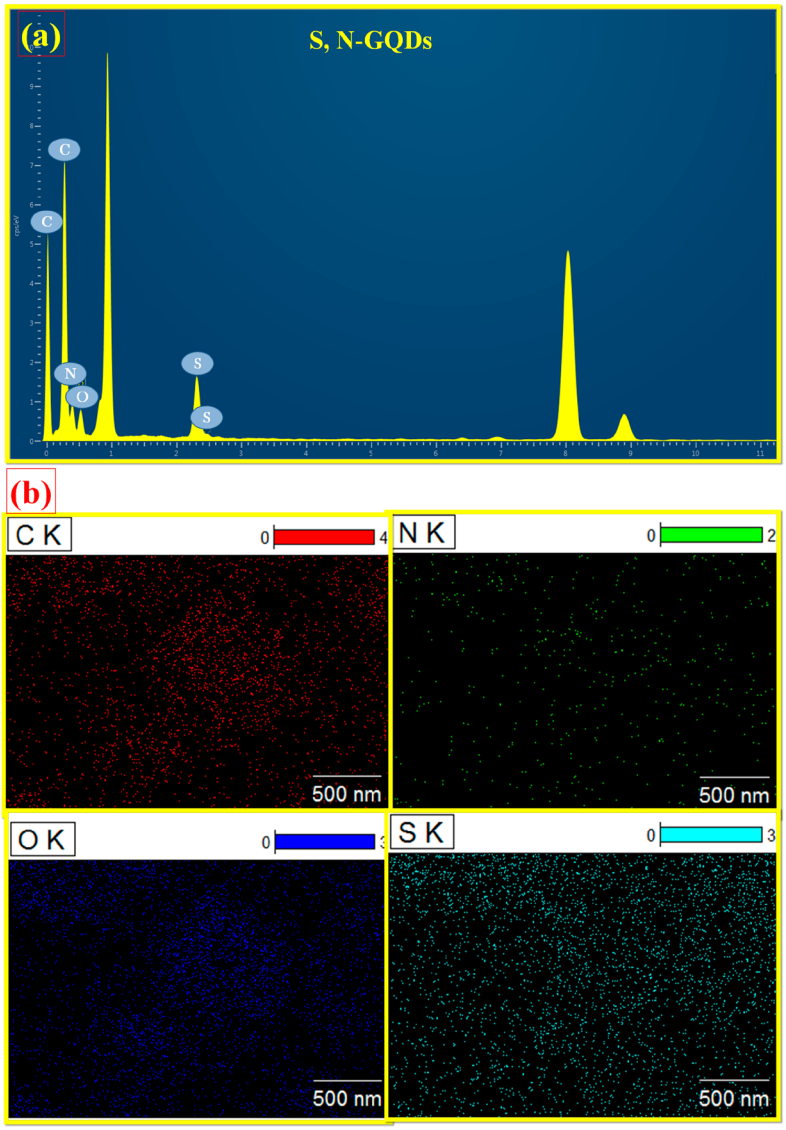

Figure 3. (a) SEM-EDAX image and (b) TEM elemental mapping image of S,N-GQDs.

https://doi.org/10.1021/acsomega.2c00092
ACS Omega 2022, 7, 12825−12834

Table 1. Atomic Percentage of the Prepared S,N-GQDs

element	line type	k factor	k factor type	absorption correction	wt %	wt % sigma	atomic %
C	K series	2.769		1.00	73.37	1.19	81.05
N	K series	3.515		1.00	10.49	1.16	9.93
O	K series	2.020		1.00	5.62	0.56	4.66
S	K series	1.000		1.00	10.52	0.47	4.35
Total:					100.00		100.00

absorption spectroscopy is often performed in the region of 4000 to 400 cm^{-1} since most organic compounds absorb radiation in this range. Figure 4 depicts the FT-IR spectra of

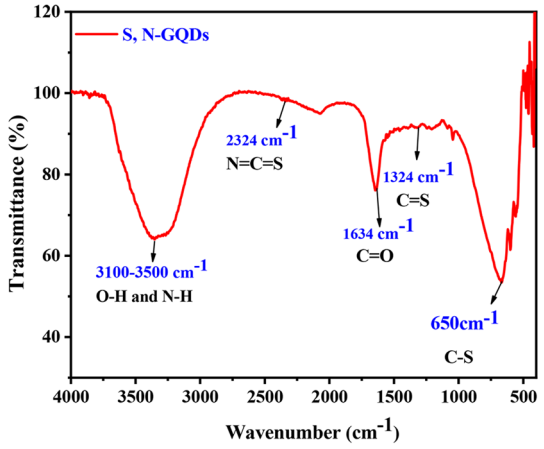

Figure 4. FT-IR spectra of the prepared S,N-GQDs.

S,N-GQDs. The stretching vibration of O−H and N−H bonds correlates to a large absorption peak around 3000−3500 cm^{-1}.[39,40] The C═O stretching vibration appears at 1634 cm^{-1}.[17] Two small peaks at 1318 and 1215 cm^{-1} arise due to asymmetric and symmetric stretching vibrations of C−O−C. The stretching modes of N═C═S are indicated by the peak at 2070 cm^{-1}. C−S stretching vibration causes the peak at 650 cm^{-1},[40] and this study clearly confirms that the synthesized compound contains both nitrogen and sulfur.

UV−vis and PL spectroscopy methods were used to characterize the optical characteristics of S,N-GQDs as shown in Figure 5a,b. The prepared S,N-GQDs exhibit significant absorption in the UV region. The absorption spectrum in Figure 5a shows two typical peaks: the first at 232 nm, corresponding to $\pi-\pi^*$ transitions of the aromatic sp^2 domains.[41] The peaks at ∼333 nm corresponding to $n-\pi^*$ transitions are due to sulfur, nitrogen, and oxygen present in the graphitic structure, which is a unique characteristic of graphene-like structures.[40] The PL spectra of the S,N-GQDs resulted as the excitation wavelength increased from 220 to 520 nm. When excited at 340 nm, the resulting S,N-GQDs have the maximum emission intensity at 448 nm as given in Figure 5b. Using DRS-UV spectroscopy, band gaps of prepared S,N-GQDs and GQDs (without doping) were estimated to be around ∼2.54 eV and ∼3.07 eV. Figure 5c reveals that sulfur and nitrogen of prepared samples reduced the band gap of GQDs, so it can be utilized for photocatalytic activities.

Photostability. A sample of the prepared S,N-GQD material showed very good fluorescence stability under UV irradiation. Figure 6 shows the comparison of the relative fluorescence intensities for S,N-GQDs over a time of 90 min under continuous excitation at 365 nm from a xenon lamp. These highly photostable S,N-GQDs will be useful for a variety of applications since their fluorescence intensity decreases by almost 1.9% under continuous xenon lamp illumination for 90 min.[42−44]

2.2. Photocatalytic Application. The coating content of S and N has a strong influence on the photocatalytic activity of the prepared S,N-GQDs. As a result, we conducted experiments to investigate how the doping content of S and N affects the ability of GQDs to remove dye under visible-light irradiation, and a doping of S and N can absorb more light energy and increase the utilization of light as well as inhibit the recombination efficiency of photogenerated charges and transfer the photogenerated charges to the reaction sites of the photocatalysts. The excess of N and S will weaken the function of GQDs for light absorption and electron pathways, and then the rate of recombination will increase for photogenerated charges. Additionally, the proper amount of doping increases light absorption and serves as an electron sink to speed up electron migration efficiency. The photocatalytic experiment was repeated using a fixed dosage of catalyst (500 μL) and varying concentrations of crystal violet and alizarin yellow dyes (20 ppm, 30 ppm, 40 ppm, and 50 ppm). In the dye degradation process, we fixed the incubation time for a total period of 100 min.

According to Figure 7a,b, photocatalytic removal of dye was decreased with increasing dye concentration and shows the effect of initial crystal violet (cationic dye) and alizarin yellow (anionic dye) dye degradation efficiency. At low concentrations, the degradation ratio increased, and then it decreased at high concentrations, as illustrated in Figure 7c,d, and shows that the increment of concentration of both dyes decreases the dye degradation % at constant time. This might be due to dye sensitization. Few dye molecules can be adsorbed on the S,N-GQD surface at low concentrations; therefore, the photo-induced charges are mostly generated by S,N-GQD excitons. The adsorption became considerable as the concentration of dyes increased. Many photoexcited electrons on adsorbed dye molecules transferred to S,N-GQDs under visible-light illumination. Initial decolorization of dye solutions with photocatalysts was minimal in dark conditions, but when we passed visible light on the dye solutions, the process became more gradual. The above statement implies that the prepared sample S,N-GQD is less potent in the dark (without light) and highly effective in visible-light conditions for dye degradation. The prepared photocatalyst was more suitable for cationic dyes like crystal violet than anionic dyes like alizarin yellow. As calculated by the dye degradation percentage after 100 min of light illumination, the crystal violet dye degraded up to 91%, and the alizarin yellow dye degraded up to 64%. In Table 2, we included the dye degradation efficiency compared with previous works done on crystal violet dye degradation. This might be due to the S,N-GQD presence of N, S, and O atoms as these elements have high electron density, so cationic dyes can interact easily and degrade with S,N-GQDs and then the

https://doi.org/10.1021/acsomega.2c00092
ACS Omega 2022, 7, 12825−12834

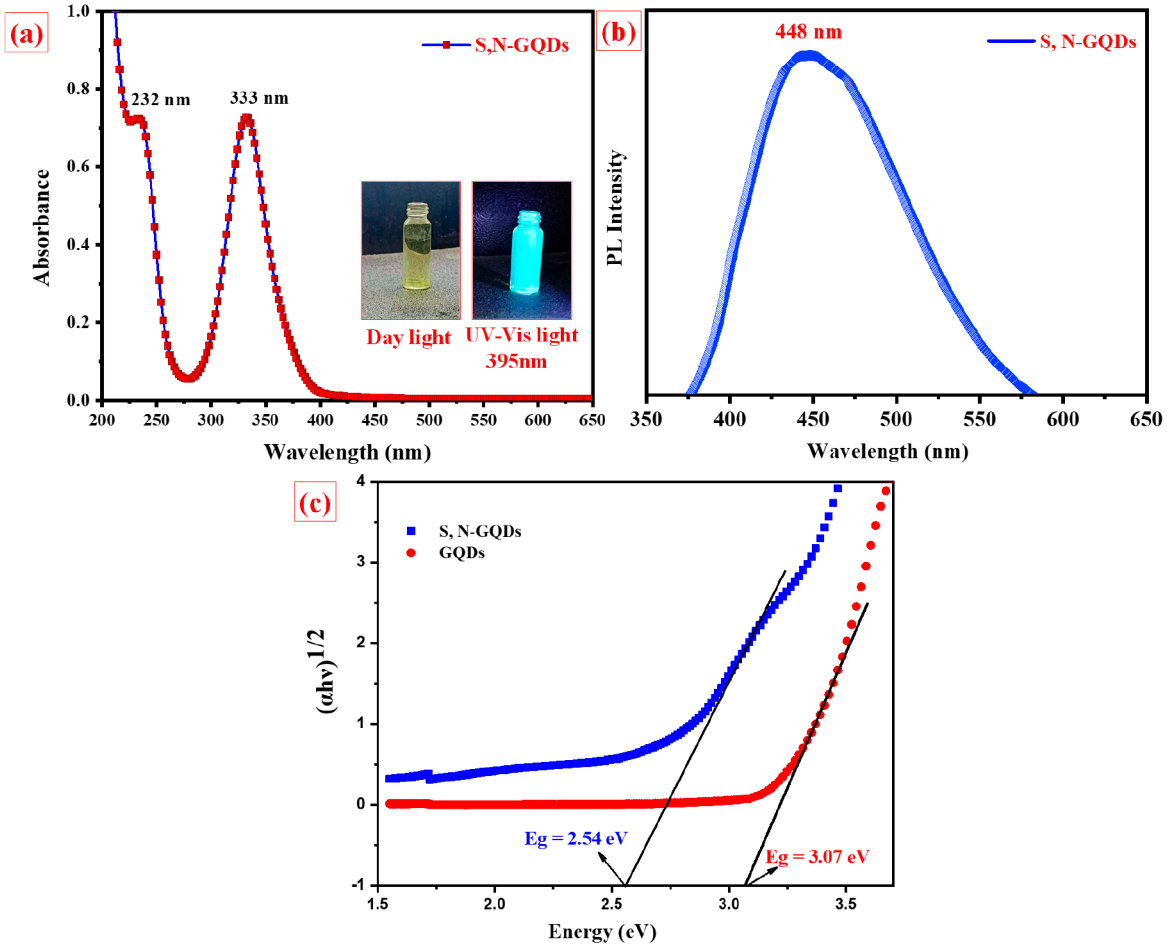

Figure 5. (a,b) UV spectra and PL spectra of S,N-GQDs. (c) Tauc plot for the estimation of band gap values of S,N-GQDs and GQDs.

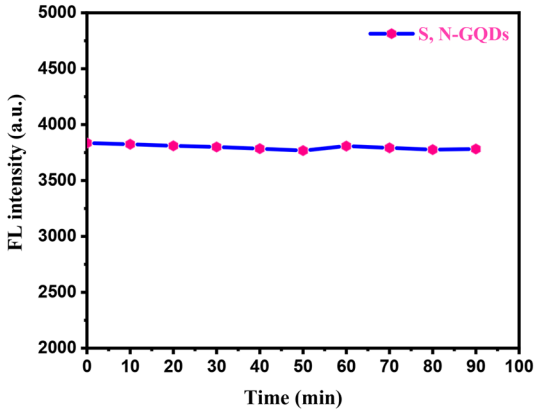

Figure 6. Photostability of the S,N-GQD solution under continuous lighting with a 365 nm UV lamp for 90 min.

anionic dye probably due to repulsion forces. From Figure 8a,b, pseudo-first-order kinetics was observed in the dye degradation process ($R^2 \sim 0.9960$).

Based on the scavenger study, we identified the species that carried out this process of photocatalysis. In this study, a variety of scavengers were employed to trap various species, including *para*-benzoquinone (BQ) which was used to indicate the $^{\bullet}O_2$ radical scavenger,[31] tertiary butyl alcohol (TBA) which was used as an OH radical scavenger,[41] and sodium salt of ethylenediaminetetraacetate (EDTA-2Na) which was used as a hole scavenger.[45] By adding these three species, we observe a significant reduction in photocatalytic efficiency, suggesting that all three of these species are involved in the photocatalysis reaction, as shown in Figure 8c. Additionally, we related the photocatalytic activity of undoped GQDs that photodegraded up to 52% of dye solution in 100 min, which is shown in Figure 8d. S,N-free GQDs have a relatively low absorbance of visible light, and their energy levels do not match those of the dye molecules, which is one of the possible explanations for their poor photodegradation efficiency.

The degraded products were examined using a total organic carbon (TOC) analyzer throughout a 100 min degradation period to see whether the decrease in absorbance was caused by a simple decolorization process given in Figure 9. The TOC value represents the amount of organics present in a solution and can be used to estimate the degree of decomposition of organic dyes. The TOC concentrations of crystal violet and alizarin yellow were 12.4% and 42.8%, respectively, when S,N-GQDs were used as a photocatalyst.

2.3. Photodegradation Mechanism. As a result of the above description, Figure 10 depicts the photocatalytic pathway of S,N-GQDs when exposed to visible light. According to the illustration, when treated with visible light, the electrons on the highest occupied molecular orbital (HOMO) level of S,N-GQDs are excited and transit to the lowest unoccupied molecular orbital (LUMO) level, while photoinduced holes remain on the HOMO level. As a result of the photoexcited electrons on the LUMO level of S,N-GQDs,

https://doi.org/10.1021/acsomega.2c00092
ACS Omega 2022, 7, 12825−12834

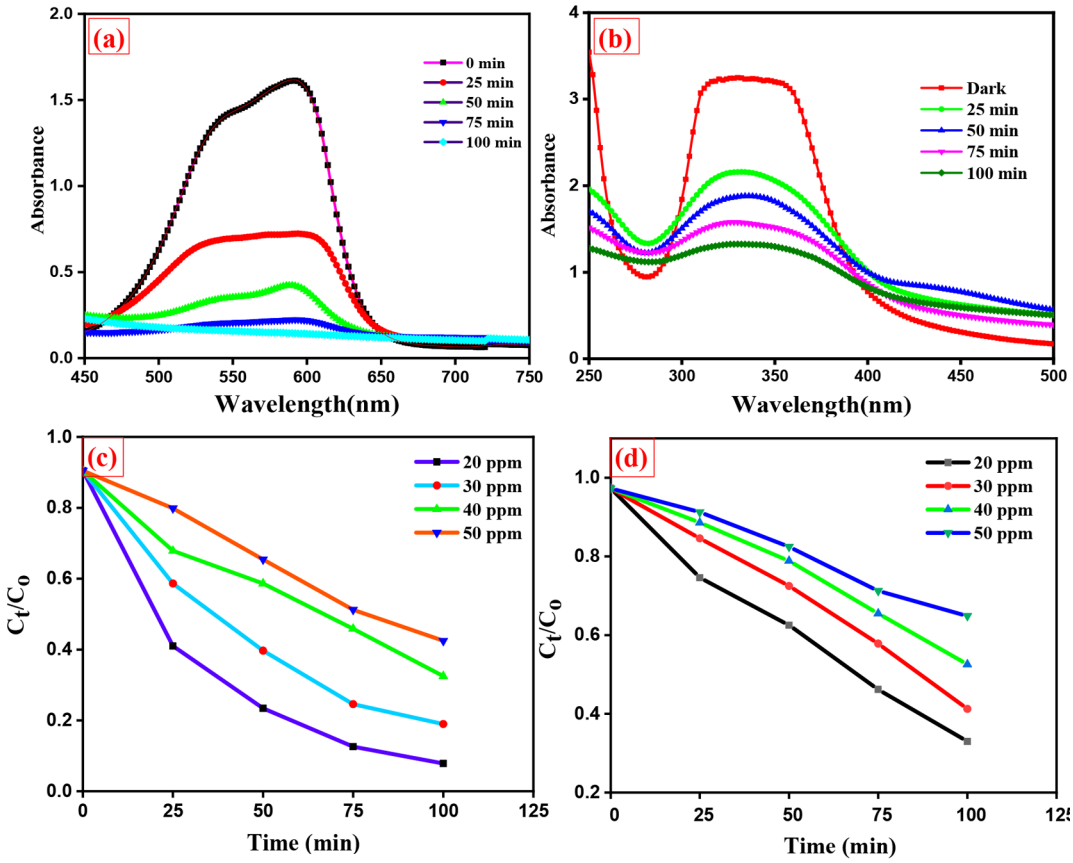

Figure 7. UV-absorption spectra of (a) crystal violet dye degradation and (b) alizarin yellow dye degradation. (c,d) The comparison of dye degradation % of various concentrations of crystal violet and alizarin yellow dye.

Table 2. Comparative Study of Crystal Violet Dye Degradation with Current and Previous Work

S. no	catalyst	dye	conc. (ppm)	degradation %	time (min)	light source	ref
1	TiO_2(B)/fullerene	crystal violet	30	82	120	visible light	46
2	Gd-doped BFO	crystal violet	20	84.4	-	visible light	47
3	$La_{1-x}Co_xCr_{1-y}Fe_yO_3$/r-GO	crystal violet	-	89.08	90	solar light	48
4	NCQGs/H_2O_2	crystal violet	10	74	150	visible light	49
5	CQDs/$KNbO_3$	crystal violet	-	70	300	visible light	50
6	AgBr-ZnO	crystal violet	10	86.93	50	visible light	51
7	$ZnTiO_3$@S	crystal violet	10	93	180	sunlight	52
8	**S,N-GQDs**	**crystal violet**	**20**	**91**	**100**	**visible light**	**current work**

the adsorbed O_2 is reduced to a radical of the type $\bullet O_2^-$, which can then be converted to another radical of the type •OH. Finally, the three kinds of active species that decompose crystal violet and alizarin yellow dyes are H^+, O_2^+, and O_2.

$$\text{S, N-GQD} + h\nu \rightarrow e^- + h^+ \quad (1)$$

$$H_2O + h^+ \rightarrow OH^{\cdot} + H^+ \quad (2)$$

$$DYE - H + h^+ \rightarrow DYE - H^{\cdot} \rightleftharpoons DYE^{\cdot} + H^+ \quad (3)$$

$$DYE^{\cdot} + O_2 \rightarrow DYE - O - O^{\cdot} \xrightarrow{H_2O/O_2} \text{degradation} \quad (4)$$

$$DYE - H + OH^{\cdot} \rightarrow H - DYE - OH^{\cdot} \xrightarrow{H_2O/O_2} \text{Degradation} \quad (5)$$

2.4. Fluorescent Security Ink Application. When short UV light (362 nm) is passed through the freshly synthesized S,N-GQDs, green color emission occurs, and when longer UV light (395 nm) is delivered through the sample, blue color emission occurs. So, it is used to prepare fluorescent ink for imaging and security purposes. Whatever we write on the paper or floor with this fluorescent ink-filled pen, it is invisible in daylight and visible light, whereas when UV light is passed on the surface of what we wrote, it emits blue or green color depending on the wavelength of UV light source as shown in Figure 11. This invisible ink is used to write any confidential matter for security purposes. Furthermore, this bright ink can be used in printing technologies on a commercial scale. For business use, this fluorescent ink pen was simple to use, inexpensive, and easy to refill.

https://doi.org/10.1021/acsomega.2c00092
ACS Omega 2022, 7, 12825−12834

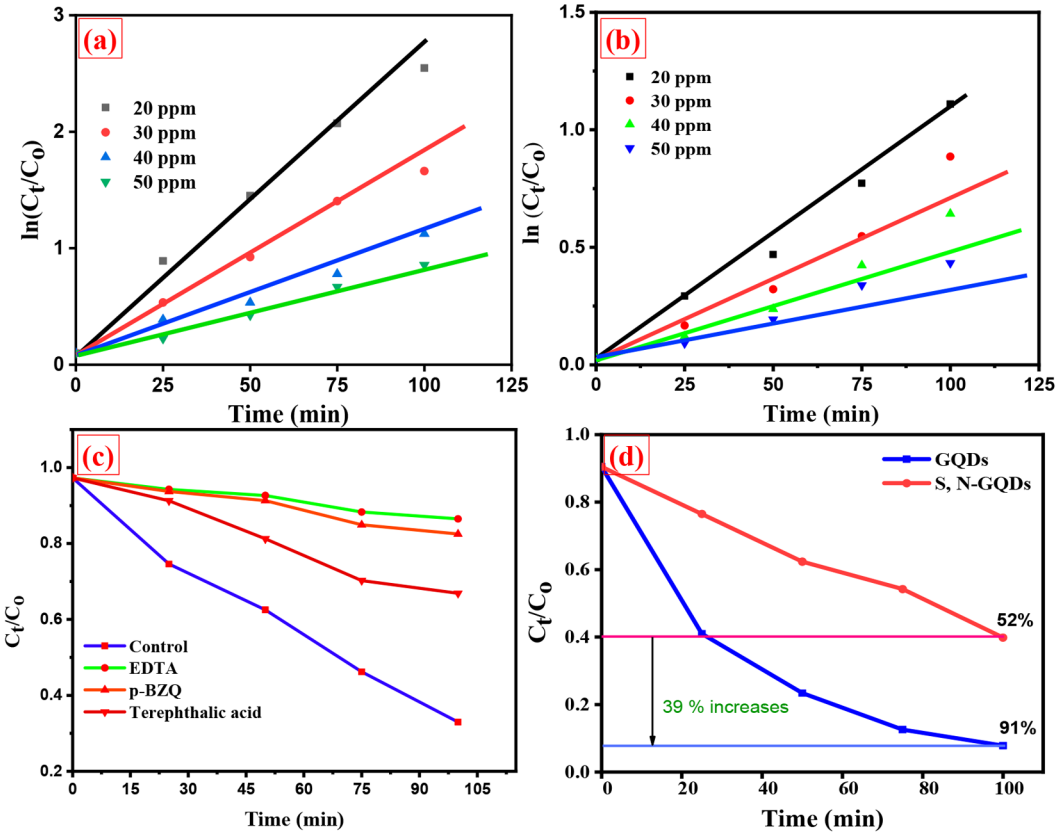

Figure 8. (a,b) Kinetic diagram for crystal violet and alizarin yellow dye with various concentrations of dye solution and (c,d) scavenger study for dye degradation and comparison of S,N-GQDs and S,N-free GQDs.

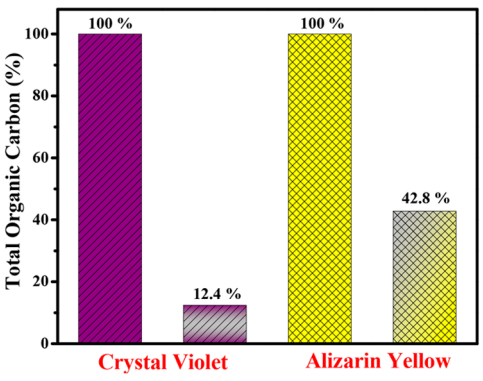

Figure 9. Total organic carbon degradation efficiency of crystal violet and alizarin yellow.

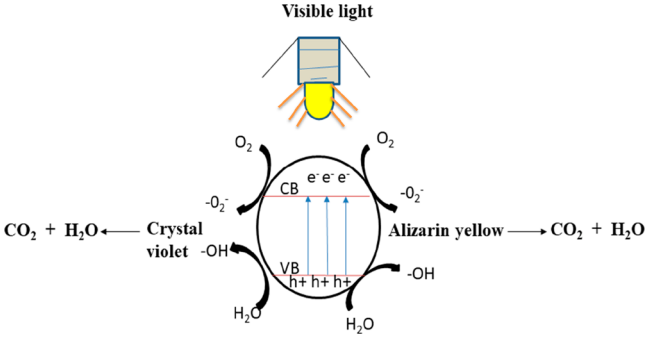

Figure 10. Photocatalytic pathway of S,N-GQDs under visible-light irradiation.

3. CONCLUSION

In this work, we prepared a highly active metal-free green nanophotocatalyst by using starch and thiourea via the hydrothermal method. The prepared compound was characterized by using TEM, EDX, FT-IR, UV−vis, and PL techniques. The synthesized S,N-GQDs have good optical and photocatalytic activity. The band gap of S,N-GQDs (~2.54 eV) was detected by using UV spectroscopy, and the broad absorption in the visible region of S,N-GQDs results in use of a photocatalyst for degradation of organic dyes such as crystal violet and alizarin yellow. The degradation percentage of crystal violet obtained was up to 91%, and for Alizarin yellow it was up to 64% within 100 min. This is a very efficient catalyst compared with S,N-free GQDs. The dopants (S, N) increased the photocatalytic activity of the prepared compound, and we also explained the mechanism of photocatalytic dye degradation by closely studying the reaction mechanism of dye degradation and observed that the photogenerated hole has a major role in dye degradation. It was dominating than the other radicals, and we have prepared a cost-effective, environmentally friendly, reusable fluorescent ink pen by using these highly luminescent graphene quantum dots that may be used for security and imaging purposes.

4. EXPERIMENTAL SECTION

4.1. Materials. Starch, thiourea (CH_4N_2S), polyvinylpyrrolidone (PVP), ethanol (C_2H_5OH), crystal violet, and alizarin yellow dye were purchased from SRL Chemicals (Chennai,

https://doi.org/10.1021/acsomega.2c00092
ACS Omega 2022, 7, 12825−12834

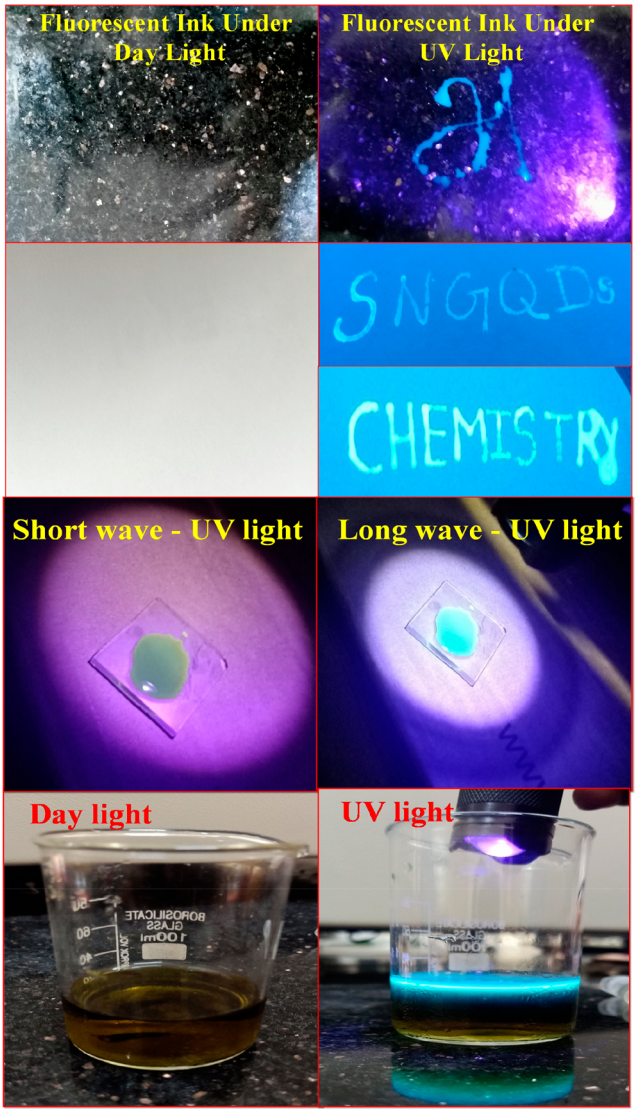

Figure 11. Text written on ordinary filter paper using an S,N-GQD fluorescent ink pen under daylight and UV light.

India). The reagents and chemicals used in these experiments were analytical grade and did not require further purification. Deionized water (DI) was utilized throughout the experiment.

4.2. Synthesis of S,N-Codoped GQDs. The preparation of S,N-GQDs is started by dissolving 5 mmol (0.525 g) of starch and 5 mmol (0.3806 g) of thiourea in 60 mL of deionized water and then stirred for 30 min under the temperature of 50 °C. Then the prepared homogeneous solution was transferred into a 100 mL Teflon-lined autoclave and maintained at 180 °C for 8 h. The prepared S,N-GQDs were collected by centrifugation at 6000 rpm for 10 min. The formation of the S,N-codoped graphene quantum dot is indicated by the finally collected brown colored supernatant, which is referred to as S,N-GQD in this study.

4.3. Preparation of Fluorescent ink. Ultrasonic treatment was used to dissolve 10 mL of the S,N-GQD sample in 15 mL of 5% polyvinylpyrrolidone (PVP) for 15 min. After magnetically stirring this mixture for 1 h, a high viscosity ink was formed. Following that, the prepared ink was poured in an empty refill tube and handwritten or drawn on regular filter paper before being left to dry in the air. We investigated the paper under UV light at 365 nm after it had dried for an hour and captured visible images, as shown in Figure 8.

4.4. Characterization Studies. The synthesized S,N-GQDs were analyzed by powder X-ray diffraction using a Rigaku Ultima III device with Cu Kα radiation, having a characteristic wavelength of λ = 1.5406 Å, and the results were collected over a scanning range of 2Θ = 10° to 80°. Using diffuse reflectance spectroscopy (DRS), we measured the UV−visible reflectivity of the synthesized photocatalyst at room temperature on a Shimadzu, UV 3600 plus in the wavelength range of 200−800 nm. The samples were then examined using transmission electron microscopy (model: TEM, 2100 electron microscopy), and also energy-dispersive X-ray analysis (EDAX) and elemental mapping were studied for elemental analysis in TEM.

4.5. Photocatalytic Experiments. The model pollutant selected for evaluating the performance of the synthesized photocatalyst is crystal violet ($C_{25}N_3H_{30}Cl$) and Alizarin yellow ($C_{14}H_8O_4$). An amount 500 μL of prepared sample was mixed into a 50 mL solution of Alizarin yellow (20 ppm) and crystal violet (20 ppm) dyes separately. Photocatalysts were not treated before being dispersed in Alizarin yellow and crystal violet solutions. The solution was then exposed to visible light using a 400 W xenon lamp for 100 min. Every 25 min, a 3 mL dye sample was collected to evaluate the concentration of dye solution using a UV−vis spectrophotometer. The degradation efficiency can be calculated as

$$\text{dye degradation (\%)} = C_o - C_t/C_o \times 100$$

where C_o denotes the concentration of dye at the time (t) = 0 s (initial) and C_t represents the concentration of dye at the final stage (time (t) = t s).

AUTHOR INFORMATION

Corresponding Author

Arulmozhi Rajaram − *Department of Chemistry, SRM Institute of Science and Technology, Kattankulathur 603203 Tamil Nadu, India;* orcid.org/0000-0001-9924-0888; Email: arulmozr@srmist.edu.in

Authors

Tamizharasan Selvakumar − *Department of Chemistry, SRM Institute of Science and Technology, Kattankulathur 603203 Tamil Nadu, India*

Muralidharan Rajaram − *Department of Physics, Saveetha School of Engineering, Saveetha Institute of Medical and Technical Sciences, Thandalam, Chennai 602105, India;* orcid.org/0000-0003-1224-2325

Abirami Natarajan − *Department of Chemistry, SRM Institute of Science and Technology, Kattankulathur 603203 Tamil Nadu, India*

Leelavathi Harikrishnan − *Department of Chemistry, SRM Institute of Science and Technology, Kattankulathur 603203 Tamil Nadu, India*

Kumarasamy Alwar − *Department of Chemistry, SRM Institute of Science and Technology, Kattankulathur 603203 Tamil Nadu, India*

Complete contact information is available at: https://pubs.acs.org/10.1021/acsomega.2c00092

Author Contributions

S. Tamilarasan: Methodology, Software, Writing - original draft, Visualization, Investigation. R. Muralidharan: Formal

https://doi.org/10.1021/acsomega.2c00092
ACS Omega 2022, 7, 12825−12834

analysis, Writing − Review & Editing. N. Abirami: Validation. H. Leelavathi, and A. Kumarasamy: Data curation. R. Arulmozhi: Conceptualization, Writing − Review & Editing, Supervision.

Notes

The authors declare no competing financial interest.

■ ACKNOWLEDGMENTS

The authors acknowledge the financial support from the Department of Chemistry, SRM Institute of Science and Technology, Tamil Nadu 603203, India.

■ REFERENCES

(1) Ahmad, A.; Mohd-Setapar, S. H.; Chuong, C. S.; Khatoon, A.; Wani, W. A.; Kumar, R.; Rafatullah, M. Recent Advances in New Generation Dye Removal Technologies: Novel Search of Approaches to Reprocess Waste Water. *RSC Adv.* **2015**, *5*, 30801−30818.

(2) Ganesan, K.; Jothi, V. K.; Natarajan, A.; Rajaram, A.; Ravichandran, S.; Ramalingam, S. Green Synthesis of Copper Oxide Nanoparticles Decorated with Graphene Oxide for Anticancer Activity and Catalytic Applications. *Arab. J. Chem.* **2020**, *13* (8), 6802−6814.

(3) Leelavathi, H.; Abirami, N.; Muralidharan, R.; Kavitha, H. P.; Tamizharasan, S.; Sankeetha, S.; Arulmozhi, R. Sunlight-Assisted Degradation of Textile Pollutants and Phytotoxicity Evaluation Using Mesoporous ZnO/g-C3N4catalyst. *RSC Adv.* **2021**, *11* (43), 26800−26812.

(4) Yaqoob, A. A.; Mohd Noor, N. H. b.; Serra, A.; Mohamad Ibrahim, M. N. Advances and Challenges in Developing Efficient Graphene Oxide-Based ZnO Photocatalysts For Dye Photo-Oxidation. *Nanomaterials* **2020**, *10*, 932.

(5) Kumar, S.; Dhiman, A.; Sudhagar, P.; Krishnan, V. ZnO-Graphene Quantum Dots Heterojunctions for Natural Sunlight-Driven Photocatalytic Environmental Remediation. *Appl. Surf. Sci.* **2018**, *447*, 802−815.

(6) Sampurnam, S.; Muthamizh, S.; Dhanasekaran, T.; Latha, D.; Padmanaban, A.; Selvam, P.; Stephen, A.; Narayanan, V. Synthesis and Characterization of Keggin-Type Polyoxometalate/Zirconia Nanocomposites—Comparison of Its Photocatalytic Activity towards Various Organic Pollutants. *J. Photochem. Photobiol. A Chem.* **2019**, *370*, 26−40.

(7) Kumaresan, A.; Arun, A.; Kalpana, V.; Vinupritha, P.; Sundaravadivel, E. Polymer-Supported NiWO4 Nanocomposites for Visible Light Degradation of Toxic Dyes. *J. Mater. Sci. Mater. Electron.* **2022**, DOI: 10.1007/s10854-021-07643-2.

(8) Ghodbane, H.; Hamdaoui, O. Decolorization of Antraquinonic Dye, C.I. Acid Blue 25, in Aqueous Solution by Direct UV Irradiation, UV/H2O2 and UV/Fe(II) Processes. *Chem. Eng. J.* **2010**, *160* (1), 226−231.

(9) Monisha, K.; Kavipriya, S.; Silambarasan, A.; Arulmozhi, R.; Abirami, N.; Ramesh, R. Hydrothermal Synthesis of Hierarchically Structured Cobalt Doped Bismuth Tungstate with Improved Photocatalytic Activity. *Optik (Stuttg).* **2020**, *206*, 164366.

(10) Sheik Mydeen, S.; Raj Kumar, R.; Sivakumar, R.; Sambathkumar, S.; Kottaisamy, M.; Vasantha, V. S. Graphene Quantum Dots/ZnO Nanocomposite: Synthesis, Characterization, Mechanistic Investigations of Photocatalytic and Antibacterial Activities. *Chem. Phys. Lett.* **2020**, *761*, 138009.

(11) Dejpasand, M. T.; Saievar-Iranizad, E.; Bayat, A.; Montaghemi, A.; Ardekani, S. R. Tuning HOMO and LUMO of Three Region (UV, Vis and IR) Photoluminescent Nitrogen Doped Graphene Quantum Dots for Photodegradation of Methylene Blue. *Mater. Res. Bull.* **2020**, *128* (April), 110886.

(12) Guo, Z.; Wu, H.; Li, M.; Tang, T.; Wen, J.; Li, X. Phosphorus-Doped Graphene Quantum Dots Loaded on TiO2 for Enhanced Photodegradation. *Appl. Surf. Sci.* **2020**, *526* (May), 146724.

(13) Yan, Y.; Gong, J.; Chen, J.; Zeng, Z.; Huang, W.; Pu, K.; Liu, J.; Chen, P. Recent Advances on Graphene Quantum Dots: From Chemistry and Physics to Applications. *Adv. Mater.* **2019**, *31* (21), 1−22.

(14) Chen, W.; Li, D.; Tian, L.; Xiang, W.; Wang, T.; Hu, W.; Hu, Y.; Chen, S.; Chen, J.; Dai, Z. Synthesis of Graphene Quantum Dots from Natural Polymer Starch for Cell Imaging. *Green Chem.* **2018**, *20* (19), 4438−4442.

(15) Kalkal, A.; Pradhan, R.; Kadian, S.; Manik, G.; Packirisamy, G. Biofunctionalized Graphene Quantum Dots Based Fluorescent Biosensor toward Efficient Detection of Small Cell Lung Cancer. *ACS Appl. Bio Mater.* **2020**, *3* (8), 4922−4932.

(16) Zhao, C.; Song, X.; Liu, Y.; Fu, Y.; Ye, L.; Wang, N.; Wang, F.; Li, L.; Mohammadniaei, M.; Zhang, M.; Zhang, Q.; Liu, J. Synthesis of graphene quantum dots and their applications in drug delivery. *J. Nanobiotechnol.* **2020**, *18*, 142.

(17) Qu, D.; Zheng, M.; Du, P.; Zhou, Y.; Zhang, L.; Li, D.; Tan, H.; Zhao, Z.; Xie, Z.; Sun, Z. Highly Luminescent S, N Co-Doped Graphene Quantum Dots with Broad Visible Absorption Bands for Visible Light Photocatalysts. *Nanoscale* **2013**, *5* (24), 12272−12277.

(18) Vatanpour, V.; Mousavi Khadem, S. S.; Masteri-Farahani, M.; Mosleh, N.; Ganjali, M. R.; Badiei, A.; Pourbashir, E.; Mashhadzadeh, A. H.; Tajammal Munir, M.; Mahmodi, G.; Zarrintaj, P.; Ramsey, J. D.; Kim, S. J.; Saeb, M. R. Anti-Fouling and Permeable Polyvinyl Chloride Nanofiltration Membranes Embedded by Hydrophilic Graphene Quantum Dots for Dye Wastewater Treatment. *J. Water Process Eng.* **2020**, *38*, 101652.

(19) Gan, X.; Yang, S.; Zhang, J.; Wang, G.; He, P.; Sun, H.; Yuan, H.; Yu, L.; Ding, G.; Zhu, Y. Graphite-N Doped Graphene Quantum Dots as Semiconductor Additive in Perovskite Solar Cells. *ACS Appl. Mater. Interfaces* **2019**, *11* (41), 37796−37803.

(20) Sim, Y.; Kim, S. J.; Janani, G.; Chae, Y.; Surendran, S.; Kim, H.; Yoo, S.; Seok, D. C.; Jung, Y. H.; Jeon, C.; Moon, J.; Sim, U. The Synergistic Effect of Nitrogen and Fluorine Co-Doping in Graphene Quantum Dot Catalysts for Full Water Splitting and Supercapacitor. *Appl. Surf. Sci.* **2020**, *507*, 145157.

(21) Nasrollahi, F.; Koh, Y. R.; Chen, P.; Varshosaz, J.; Khodadadi, A. A.; Lim, S. Targeting Graphene Quantum Dots to Epidermal Growth Factor Receptor for Delivery of Cisplatin and Cellular Imaging. *Mater. Sci. Eng., C* **2019**, *94*, 247−257.

(22) Freitas, F. S.; Gonçalves, A. S.; De Morais, A.; Benedetti, J. E.; Nogueira, A. F. Graphene-like MoS2 as a Low-Cost Counter Electrode Material for Dye-Sensitized Solar Cells. *J. NanoGe J. Energy Sustain.* **2012**, No. 1, 11002−11003.

(23) Safardoust-Hojaghan, H.; Salavati-Niasari, M. Degradation of Methylene Blue as a Pollutant with N-Doped Graphene Quantum Dot/Titanium Dioxide Nanocomposite. *J. Clean. Prod.* **2017**, *148*, 31−36.

(24) Hasan, M. T.; Gonzalez-Rodriguez, R.; Ryan, C.; Pota, K.; Green, K.; Coffer, J. L.; Naumov, A. V. Nitrogen-Doped Graphene Quantum Dots: Optical Properties Modification and Photovoltaic Applications. *Nano Res.* **2019**, *12* (5), 1041−1047.

(25) Huang, D.; Zhou, H.; Wu, Y.; Wang, T.; Sun, L.; Gao, P.; Sun, Y.; Huang, H.; Zhou, G.; Hu, J. Bottom-up Synthesis and Structural Design Strategy for Graphene Quantum Dots with Tunable Emission to near Infrared Region. *Carbon N. Y.* **2019**, *142*, 673−684.

(26) Ju, J.; Chen, W. Synthesis of Highly Fluorescent Nitrogen-Doped Graphene Quantum Dots for Sensitive, Label-Free Detection of Fe (III) in Aqueous Media. *Biosens. Bioelectron.* **2014**, *58*, 219−225.

(27) Li, M.; Wu, W.; Ren, W.; Cheng, H. M.; Tang, N.; Zhong, W.; Du, Y. Synthesis and Upconversion Luminescence of N-Doped Graphene Quantum Dots. *Appl. Phys. Lett.* **2012**, *101* (10), 103107.

(28) Sun, H.; Ji, H.; Ju, E.; Guan, Y.; Ren, J.; Qu, X. Synthesis of Fluorinated and Nonfluorinated Graphene Quantum Dots through a New Top-down Strategy for Long-Time Cellular Imaging. *Chem. - A Eur. J.* **2015**, *21* (9), 3791−3797.

(29) Ge, S.; He, J.; Ma, C.; Liu, J.; Xi, F.; Dong, X. One-Step Synthesis of Boron-Doped Graphene Quantum Dots for Fluorescent Sensors and Biosensor. *Talanta* **2019**, *199*, 581−589.

https://doi.org/10.1021/acsomega.2c00092
ACS Omega 2022, 7, 12825−12834

(30) Tang, L.; Ji, R.; Li, X.; Teng, K. S.; Lau, S. P. Energy-Level Structure of Nitrogen-Doped Graphene Quantum Dots. *J. Mater. Chem. C* **2013**, *1* (32), 4908−4915.
(31) Huang, B.; He, J.; Bian, S.; Zhou, C.; Li, Z.; Xi, F.; Liu, J.; Dong, X. S-Doped Graphene Quantum Dots as Nanophotocatalyst for Visible Light Degradation. *Chin. Chem. Lett.* **2018**, *29* (11), 1698−1701.
(32) Serhan, M.; Sprowls, M.; Jackemeyer, D.; Long, M.; Perez, I. D.; Maret, W.; Tao, N.; Forzani, E. Total Iron Measurement in Human Serum with a Smartphone. *AIChE Annu. Meet. Conf. Proc.* 2019, DOI: 10.1039/x0xx00000x.
(33) Mombrú, D.; Romero, M.; Faccio, R.; Mombrú, Á. W. Electronic and Optical Properties of Sulfur and Nitrogen Doped Graphene Quantum Dots: A Theoretical Study. *Phys. E Low-Dimensional Syst. Nanostructures* **2019**, *113* (May), 130−136.
(34) Zhang, B. X.; Gao, H.; Li, X. L. Synthesis and Optical Properties of Nitrogen and Sulfur Co-Doped Graphene Quantum Dots. *New J. Chem.* **2014**, *38* (9), 4615−4621.
(35) Zhang, R.; Adsetts, J. R.; Nie, Y.; Sun, X.; Ding, Z. Electrochemiluminescence of Nitrogen- and Sulfur-Doped Graphene Quantum Dots. *Carbon N. Y.* **2018**, *129*, 45−53.
(36) Behnood, R.; Sodeifian, G. Novel ZnCo2O4 Embedded with S, N-CQDs as Efficient Visible-Light Photocatalyst. *J. Photochem. Photobiol. A Chem.* **2021**, *405*, 112971.
(37) Atchudan, R.; Edison, T. N. J. I.; Perumal, S.; Vinodh, R.; Lee, Y. R. Betel-Derived Nitrogen-Doped Multicolor Carbon Dots for Environmental and Biological Applications. *J. Mol. Liq.* **2019**, *296*, 111817.
(38) Atchudan, R.; Edison, T. N. J. I.; Lee, Y. R. Nitrogen-Doped Carbon Dots Originating from Unripe Peach for Fluorescent Bioimaging and Electrocatalytic Oxygen Reduction Reaction. *J. Colloid Interface Sci.* **2016**, *482*, 8−18.
(39) Murugan, K.; Jothi, V. K.; Rajaram, A.; Natarajan, A. Novel Metal-Free Fluorescent Sensor Based on Molecularly Imprinted Polymer N-CDs@MIP for Highly Selective Detection of TNP. *ACS Omega* **2022**, *7* (1), 1368−1379.
(40) Mondal, T. K.; Dinda, D.; Saha, S. K. Nitrogen, Sulphur Co-Doped Graphene Quantum Dot: An Excellent Sensor for Nitro-explosives. *Sensors Actuators, B Chem.* **2018**, *257*, 586−593.
(41) Saini, D.; Kaushik, J.; Garg, A. K.; Dalal, C.; Sonkar, S. K. N, S-Codoped Carbon Dots for Nontoxic Cell Imaging and As a Sunlight-Active Photocatalytic Material for the Removal of Chromium. *ACS Appl. Bio Mater.* **2020**, *3* (6), 3656−3663.
(42) Ren, Q.; Ga, L.; Ai, J. Rapid Synthesis of Highly Fluorescent Nitrogen-Doped Graphene Quantum Dots for E Ff Ective Detection of Ferric Ions and as Fluorescent Ink. *ACS Omega* **2019**, *4*, 15842.
(43) Mondal, T. K.; Saha, S. K. Article A Facile Approach to Synthesize Nitrogen and Oxygen Rich Carbon Quantum Dots for PH Sensor, Fluorescent Indicator and Invisible Ink Applications A Facile Approach to Synthesize Nitrogen and Oxygen Rich Carbon Quantum Dots for PH Sensor. *Fluoresc.* **2019**, *7*, 19669.
(44) Anand, S. R.; Bhati, A.; Saini, D.; Chauhan, N.; Khare, P.; Sonkar, S. K. Antibacterial Nitrogen-Doped Carbon Dots as a Reversible " Fluorescent Nanoswitch " and Fluorescent Ink. *ACS Omega* **2019**, *4*, 1581−1591.
(45) Aggarwal, R.; Saini, D.; Singh, B.; Kaushik, J.; Garg, A. K.; Sonkar, S. K. Bitter Apple Peel Derived Photoactive Carbon Dots for the Sunlight Induced Photocatalytic Degradation of Crystal Violet Dye. *Sol. Energy* **2020**, *197*, 326−331.
(46) Panahian, Y.; Arsalani, N.; Nasiri, R. Enhanced Photo and Sono-Photo Degradation of Crystal Violet Dye in Aqueous Solution by 3D Flower like F-TiO2(B)/Fullerene under Visible Light. *J. Photochem. Photobiol. A Chem.* **2018**, *365*, 45−51.
(47) Kossar, S.; Banu, I. B. S.; Aman, N.; Amiruddin, R. Investigation on Photocatalytic Degradation of Crystal Violet Dye Using Bismuth Ferrite Nanoparticles. *J. Dispers. Sci. Technol.* **2021**, *42* (14), 2053−2062.
(48) Aamir, M.; Bibi, I.; Ata, S.; Majid, F.; Kamal, S.; Alwadai, N.; Sultan, M.; Iqbal, S.; Aadil, M.; Iqbal, M. Graphene Oxide Nanocomposite with Co and Fe Doped LaCrO3 Perovskite Active under Solar Light Irradiation for the Enhanced Degradation of Crystal Violet Dye. *J. Mol. Liq.* **2021**, *322*, 114895.
(49) Smrithi, S. P.; Kottam, N.; Vergis, B. R. Heteroatom Modified Hybrid Carbon Quantum Dots Derived from Cucurbita Pepo for the Visible Light Driven Photocatalytic Dye Degradation. *Top. Catal.* **2022**, DOI: 10.1007/s11244-022-01581-x.
(50) Qu, Z.; Wang, J.; Tang, J.; Shu, X.; Liu, X.; Zhang, Z.; Wang, J. Carbon Quantum Dots/KNbO3 Hybrid Composites with Enhanced Visible-Light Driven Photocatalytic Activity toward Dye Waste-Water Degradation and Hydrogen Production. *Mol. Catal.* **2018**, *445*, 1−11.
(51) Abdel-Khalek, A. A.; Mahmoud, S. A.; Zaki, A. H. Visible Light Assisted Photocatalytic Degradation of Crystal Violet, Bromophenol Blue and Eosin Y Dyes Using AgBr-ZnO Nanocomposite. *Environ. Nanotechnology, Monit. Manag.* **2018**, *9*, 164−173.
(52) Tavakoli-Azar, T.; Mahjoub, A. R.; Sadjadi, M. S.; Farhadyar, N.; Sadr, M. H. Improving the Photocatalytic Performance of a Perovskite ZnTiO3 through ZnTiO3@S Nanocomposites for Degradation of Crystal Violet and Rhodamine B Pollutants under Sunlight. *Inorg. Chem. Commun.* **2020**, *119*, 108091.
(53) Atchudan, R.; Edison, T. N. J. I.; Aseer, K. R.; Perumal, S.; Karthik, N.; Lee, Y. R. Highly Fluorescent Nitrogen-Doped Carbon Dots Derived from Phyllanthus Acidus Utilized as a Fluorescent Probe for Label-Free Selective Detection of Fe3+ Ions, Live Cell Imaging and Fluorescent Ink. *Biosens. Bioelectron.* **2018**, *99*, 303−311.
(54) Atchudan, R.; Edison, T. N. J. I.; Perumal, S.; Muthuchamy, N.; Lee, Y. R. Hydrophilic Nitrogen-Doped Carbon Dots from Biowaste Using Dwarf Banana Peel for Environmental and Biological Applications. *Fuel* **2020**, *275*, 117821.
(55) Atchudan, R.; Edison, T. N. J. I.; Sethuraman, M. G.; Lee, Y. R. *Efficient Synthesis of Highly Fluorescent Nitrogen-Doped Carbon Dots for Cell Imaging Using Unripe Fruit Extract of Prunus Mume*; Elsevier B.V., 2016; Vol. *384*. DOI: 10.1016/j.apsusc.2016.05.054.
(56) Leelavathi, H.; Muralidharan, R.; Abirami, N.; Tamizharasan, S.; Kumarasamy, A.; Arulmozhi, R. Exploration of ZnO decorated g-C3N4 amphiphilic anticancer drugs for antiproliferative activity against human cervical cancer. *Journal of Drug Delivery Science and Technology* **2022**, *68*, 103126.

https://doi.org/10.1021/acsomega.2c00092
ACS Omega 2022, 7, 12825−12834